# Concealed Object Segmentation with Hierarchical Coherence Modeling

Fengyang Xiao[1,⋆][0009−0001−5770−8953], Pan Zhang[1][0009−0002−0721−4063],
Chunming He[2,†][0000−0001−6479−7109], Runze Hu[3][0000−0002−6366−3763], and
Yutao Liu[4][0000−0002−3066−1884]

[1] Sun Yat-sen University, Zhuhai, 510275, China
`xiaofy5@mail2.sysu.edu.cn`
[2] Tsinghua Shenzhen International Graduate School, Tsinghua University, Shenzhen
518055, China
`chunminghe19990224@gmail.com`
[3] Beijing Institute of Technology, Beijing, 100086, China
[4] School of Computer Science and Technology, Ocean University of China, Qingdao,
266000, China

**Abstract.** Concealed object segmentation (COS) is a challenging task that involves localizing and segmenting those concealed objects that are visually blended with their surrounding environments. Despite achieving remarkable success, existing COS segmenters still struggle to achieve complete segmentation results in extremely concealed scenarios. In this paper, we propose a Hierarchical Coherence Modeling (HCM) segmenter for COS, aiming to address this incomplete segmentation limitation. In specific, HCM promotes feature coherence by leveraging the intra-stage coherence and cross-stage coherence modules, exploring feature correlations at both the single-stage and contextual levels. Additionally, we introduce the reversible re-calibration decoder to detect previously undetected parts in low-confidence regions, resulting in further enhancing segmentation performance. Extensive experiments conducted on three COS tasks, including camouflaged object detection, polyp image segmentation, and transparent object detection, demonstrate the promising results achieved by the proposed HCM segmenter.

**Keywords:** Concealed object segmentation · Hierarchical coherence modeling · Edge reconstruction.

## 1 Introduction

Concealed object segmentation (COS) is a challenging task with the purpose of localizing and segmenting those objects visually blended in their surrounding

---

⋆ First Author, † Corresponding Author

(a) Origin          (b) GT          (c) UGTR          (d) SegMaR          (e) HCM
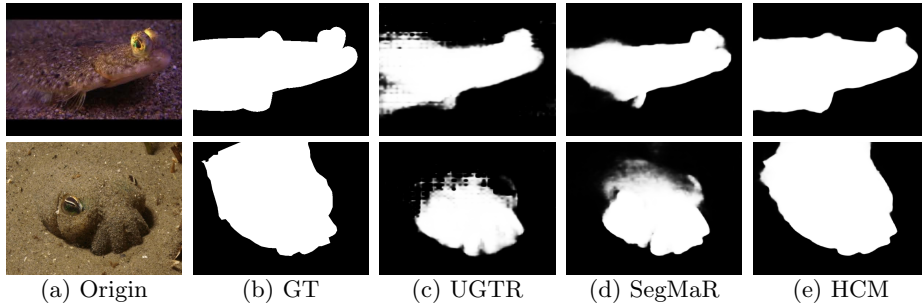
Fig. 1: Results of UGTR [36], SegMaR [17], and the proposed HCM. It is observed that our HCM can generate more accurate and complete results.

scenarios [3,10]. COS is a general task encompassing various applications, such as camouflaged object detection (COD) [3], polyp image segmentation (PIS) [4], and transparent object detection (TOD) [25].

COS poses significant challenges due to the intrinsic similarity between foreground objects and their corresponding scenarios, making it difficult to identify discriminative cues for complete and accurate foreground-background separation. To cope with this challenge, existing COS segmenters have employed various strategies, *e.g.*, drawing inspiration from human vision [24,28,11], incorporating frequency clues [9], and adopting joint modeling strategies across multiple tasks [37,22]. Despite their notable achievements, existing segmenters still struggle to achieve *precise* results in some extremely concealed scenarios. As shown in Fig. 1, while UGTR [36] and SegMaR [17] manage to find the rough regions for the concealed objects, the prediction results are still incomplete.

To overcome this limitation, we propose a Hierarchical Coherence Modeling (HCM) segmenter for the COS task, which aims to generate more complete segmentation maps by promoting feature coherence. HCM incorporates two key components, namely, intra-stage coherence (ISC) and cross-stage coherence (CSC), to explore feature correlations at both single stage and contextual levels. Additionally, we develop the reversible re-calibration decoder (RRD) to detect previously undetected parts in those low-confidence regions and thus further improve segmentation performance.

Our contributions are summarized as follows:

- We propose the Hierarchical Coherence Modeling (HCM) segmenter for the COS task. HCM encourages feature coherence and thus alleviating the incomplete segmentation problem.
- We introduce RRD to detect previously undetected parts in low-confidence regions, thus improving segmentation performance.
- The proposed HCM significantly outperforms the state-of-the-art methods on three COS tasks by a large margin, *i.e.*, camouflaged object detection, polyp image segmentation, and transparent object detection.
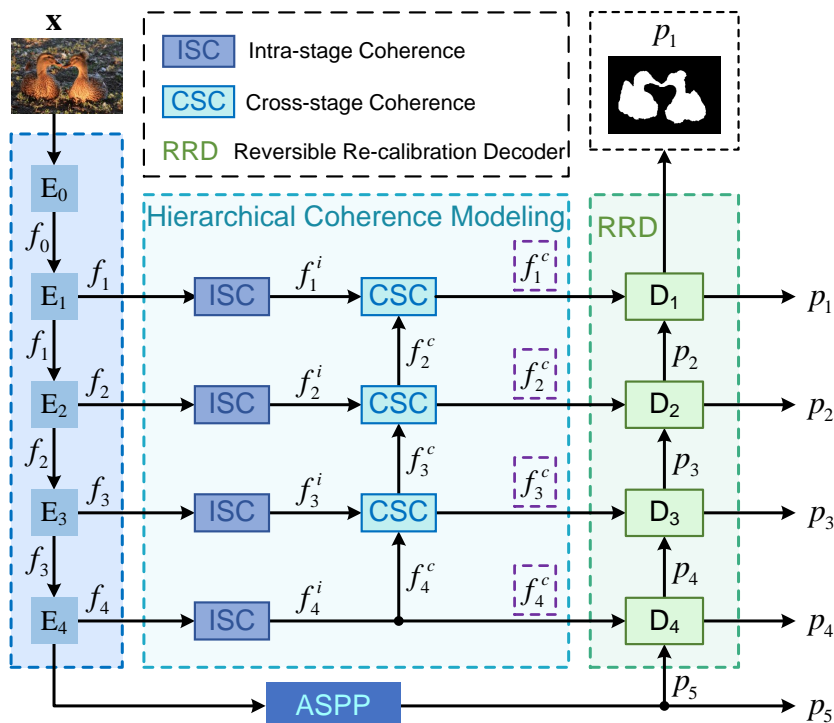
Fig. 2: Architecture of the proposed HCM.

## 2   Related Works

**Concealed Object Segmentation**. Traditional COS techniques heavily rely on manually designed feature extraction operators, which inherently suffer from limited feature extraction capacity and struggle to handle extremely complex scenarios. In contrast, learning-based approaches, facilitated by the rapid development of deep learning, have achieved remarkable success in this field. For instance, MGL [37] introduces an auxiliary edge reconstruction task and constructs a mutual graph learning strategy to generate prediction maps with clear boundaries. Inspired by human vision principles [24], PFNet leverages distraction mining techniques to achieve accurate concealed object segmentation. Recognizing the limitations of human vision, FEDER [9] introduces an adaptive decomposition approach to extract subtle yet discriminative clues that may have been overlooked. Unlike existing COS solvers, we propose HCM segmenter for the COS task, which encourages feature coherence and thus alleviates the incomplete segmentation problem. Additionally, we introduce the reversible re-calibration decoder (RRD) to detect previously undetected parts in low-confidence regions, further enhancing the segmentation performance.
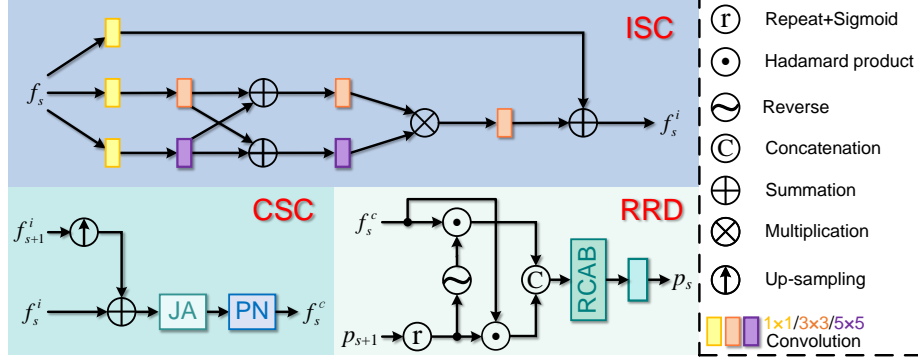
Fig. 3: Details of ISC, CSC, and RRD.

## 3 Methodology

### 3.1 Concealed Feature Encoder

Follow [3], we employ ResNet50 [14,7] as the default backbone of the basic encoder $E$ for feature extraction. Given a concealed image $\mathbf{X}$, we obtain a series of feature maps $\{f_s\}_{s=0}^{4}$. Considering that $f_4$ has abundant semantic information, we further feed this feature map into an astrous spatial pyramid pooling (ASPP) module $A_s$ [15] to generate a coarse segmentation map $p_5$: $p_5 = A_s(f_4)$.

### 3.2 Hierarchical Coherence Modeling

Due to the inherent similarity between concealed objects and their surrounding contexts, obtaining accurate and complete segmentation results poses a significant challenge for the segmenter. To address this issue, we propose a hierarchical coherence modeling strategy that explicitly promotes feature coherence to facilitate more comprehensive predictions. Illustrated in Fig. 3, this strategy consists of two parts: intra-stage coherence (ISC) and cross-stage coherence (CSC). These parts work in conjunction to enhance the coherence of features at different stages, promoting better segmentation outcomes.

**Intra-stage coherence**. ISC aims to discover feature correlations by fusing multi-scale features with different receptive fields within a single stage. This allows the aggregated features to capture scale-invariant information. As illustrated in Fig. 3, ISC comprises two primary branches with residual connections. Given the input feature $f_s$, we initially apply a $1 \times 1$ convolution to reduce the channel dimension. Subsequently, we process these features with two parallel convolutions using different kernel sizes, resulting in features $f_s^3$ and $f_s^5$:

$$f_s^3 = conv3(conv1(f_s)), f_s^5 = conv5(conv1(f_s)), \quad (1)$$

where $conv1, conv3, conv5$ denote $1 \times 1, 3 \times 3, 5 \times 5$ convolutions, respectively. We proceed by merging the features $f_s^3$ and $f_s^5$, which are obtained from the previous step. These merged features are then further processed using two parallel

convolutions. Finally, we multiply the outputs of these convolutions in a residual connection structure to extract the scale-invariant information. This process yields the aggregated features $\{f_s^i\}_{s=1}^4$:

$$f_s^i = conv1(f_s) + conv3(conv3(f_s^3 \oplus f_s^5) \otimes conv5(f_s^3 \oplus f_s^5)), \qquad (2)$$

where $\oplus$ and $\otimes$ denote pixel-level summation and multiplication. This design facilitates the extraction of features at multiple scales and enhances the ability to capture diverse contextual information.

**Cross-stage coherence**. CSC explores the contextual feature correlations by selectively interacting cross-stage information with joint attention $JA(\cdot)$, comprising spatial attention and channel attention [16,2]. Additionally, we employ position normalization $PN(\cdot)$ to highlight the contextual similarity and eliminate discrepancy interference information across different stages, getting $\{f_s^c\}_{s=1}^4$:

$$f_s^c = PN(JA(f_s^i, up(f_{s+1}^i))), \qquad (3)$$

where $up(\cdot)$ denotes up-sampling operator.

### 3.3   Reversible Re-calibration Decoder

Due to the complexity of concealed object scenes, segmenters produce prediction maps that contain low-confidence and ambiguous regions. To tackle this challenge, we propose a novel module called Reversible Re-calibration Decoder (RRD). As shown in Fig. 3, RRD leverages both the previous decoder's prediction map as prior information and reverses the prediction map to extract cues from the low-confidence regions. This allows the segmenter to effectively detect previously undetected parts in these regions, leading to improved segmentation performance. Consequently, the prediction map $\{p_s\}_{s=1}^4$ is defined as follows:

$$p_s = conv3\left(RCAB\left(cat\left(f_k^s \odot S\left(rp\left(p_{s+1}\right)\right), f_k^s \odot rv\left(S\left(rp\left(p_{s+1}\right)\right)\right)\right)\right)\right), \qquad (4)$$

where $rp(\cdot)$, $S(\cdot)$, $rv(\cdot)$, $\odot$, and $conv3(\cdot)$ denote repeat, Sigmoid, reverse (element-wise subtraction with 1), Hadamard product, and $3 \times 3$ convolution. $RCAB(\cdot)$ is the residual channel attention block [34,18] and we employ this block to emphasize the noteworthy information.

### 3.4   Loss Functions

We follow the practice in [3,9] and employ the weighted binary cross-entropy loss $L_{BCE}^w$ [35] and weighted intersection-over-union loss $L_{IoU}^w$ [29] to supervised our HCM with the ground truth $\mathbf{Y}$ in a multiscale manner ,which is defined as follows:

$$L = \sum_{s=1}^5 \frac{1}{2^{s-1}}\left(L_{BCE}^w\left(p_s, \mathbf{Y}\right) + L_{BCE}^w\left(p_s, \mathbf{Y}\right)\right) + L_{OH}. \qquad (5)$$

## 4   Experiments

**Implementation details**. Our HCM is implemented on two RTX3090TI GPUs and is optimized by Adam with the momentum terms $(0.9, 0.999)$. Following [3],

Table 1: Quantitative comparisons of our method and other 9 ResNet50-based SOTAs on COD. The best two results are in **red** and **blue** fonts.

| Methods | Pub. | CAMO (250 images) | | | | COD10K (2,026 images) | | | | NC4K (4,121 images) | | | |
|---|---|---|---|---|---|---|---|---|---|---|---|---|---|
| | | $M \downarrow$ | $F_\beta \uparrow$ | $E_\phi \uparrow$ | $S_\alpha \uparrow$ | $M \downarrow$ | $F_\beta \uparrow$ | $E_\phi \uparrow$ | $S_\alpha \uparrow$ | $M \downarrow$ | $F_\beta \uparrow$ | $E_\phi \uparrow$ | $S_\alpha \uparrow$ |
| PFANet [40] | CVPR19 | 0.132 | 0.607 | 0.701 | 0.695 | 0.074 | 0.478 | 0.729 | 0.716 | 0.095 | 0.634 | 0.760 | 0.752 |
| CPD [32] | CVPR19 | 0.113 | 0.675 | 0.723 | 0.716 | 0.053 | 0.578 | 0.776 | 0.750 | 0.072 | 0.719 | 0.808 | 0.787 |
| EGNet [39] | ICCV19 | 0.109 | 0.667 | 0.800 | 0.732 | 0.061 | 0.526 | 0.810 | 0.736 | 0.075 | 0.671 | 0.841 | 0.777 |
| SINet [3] | CVPR20 | 0.092 | 0.712 | 0.804 | 0.745 | 0.043 | 0.667 | 0.864 | 0.776 | 0.058 | 0.768 | 0.871 | 0.808 |
| PFNet [24] | CVPR21 | 0.085 | 0.751 | 0.841 | 0.782 | 0.040 | 0.676 | 0.877 | 0.800 | 0.053 | 0.779 | 0.887 | 0.829 |
| MGL-R [37] | CVPR21 | 0.088 | 0.738 | 0.812 | 0.775 | **0.035** | 0.680 | 0.851 | 0.814 | 0.053 | 0.778 | 0.867 | 0.833 |
| MGL-S [37] | CVPR21 | 0.089 | 0.733 | 0.806 | 0.772 | 0.037 | 0.666 | 0.844 | 0.811 | 0.055 | 0.771 | 0.862 | 0.829 |
| LSR [23] | CVPR21 | 0.080 | 0.756 | 0.838 | 0.787 | 0.037 | **0.699** | 0.880 | 0.804 | 0.048 | **0.802** | **0.890** | 0.834 |
| UGTR [36] | ICCV21 | 0.086 | 0.747 | 0.821 | 0.784 | 0.036 | 0.670 | 0.852 | **0.817** | **0.052** | 0.778 | 0.874 | **0.839** |
| SegMaR [17] | CVPR22 | **0.072** | **0.772** | **0.861** | **0.805** | **0.035** | **0.699** | **0.890** | 0.813 | **0.052** | 0.767 | 0.885 | 0.835 |
| HCM (Ours) | — | **0.070** | **0.782** | **0.873** | **0.806** | **0.032** | **0.736** | **0.902** | **0.820** | **0.046** | **0.816** | **0.900** | **0.846** |



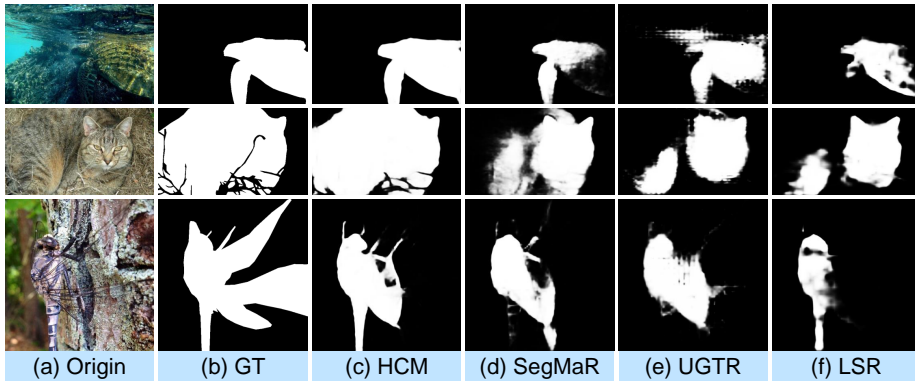(a) Origin      (b) GT      (c) HCM      (d) SegMaR      (e) UGTR      (f) LSR

Fig. 4: Qualitative analysis on the COD task.

our encoder is initialized with the model pre-trained on ImageNet. During the training phase, the batch size is set to 32. The learning rate is initialized to 0.0001 and is divided by 10 every 80 epochs. The images are resized as $352 \times 352$.

### 4.1   Camouflaged Object Segmentation

**Datasets and metrics**. Following [17], three datasets are utilized for evaluation, including *CAMO*, *COD10K*, and *NC4K*. *CAMO* comprises 1,250 camouflaged images with 8 categories. *COD10K* have 10 super-classes, containing 5,066 images. *NC4K* is the largest testing set which contains 4,121 images. Same as existing methods [3,17], our training set comprises 1,000 images from *CAMO* and 3,000 images from *COD10K*, and our test set integrates the rest of images.

Following [3,12], we utilize four metrics, namely mean absolute error $M$, adaptive F-measure $F_\beta$, mean E-measure $E_\phi$, and structure measure $S_\alpha$. Smaller $M$ means better performance, yet this is reversed on $F_\beta$, $E_\phi$, and $S_\alpha$.

**Quantitative analysis.** We compare the proposed Hierarchical Coherence Model (HCM) with nine other state-of-the-art ResNet50-based segmenters on the COD

Table 2: Quantitative comparisons on two benchmarks in polyp image segmentation. The best two results are in **red** and **blue** fonts.

| Methods | CVC-ColonDB (380 images) | | | | | | Kvasir (100 images) | | | | | |
|---|---|---|---|---|---|---|---|---|---|---|---|---|
| | mDice ↑ | mIoU ↑ | $M$ ↓ | $F_\beta^w$ ↑ | $E_\phi^{max}$ ↑ | $S_\alpha$ ↑ | mDice ↑ | mIoU ↑ | $M$ ↓ | $F_\beta^w$ ↑ | $E_\phi^{max}$ ↑ | $S_\alpha$ ↑ |
| U-Net [30] | 0.512 | 0.444 | 0.061 | 0.498 | 0.776 | 0.712 | 0.818 | 0.746 | 0.055 | 0.794 | 0.893 | 0.858 |
| Atten-UNet [27] | 0.466 | 0.385 | 0.071 | 0.431 | 0.724 | 0.670 | 0.769 | 0.683 | 0.062 | 0.730 | 0.859 | 0.828 |
| SFA [5] | 0.469 | 0.347 | 0.094 | 0.379 | 0.765 | 0.634 | 0.723 | 0.611 | 0.075 | 0.670 | 0.849 | 0.782 |
| PraNet [4] | 0.709 | 0.640 | 0.045 | 0.696 | 0.869 | 0.819 | 0.898 | 0.840 | 0.030 | 0.885 | 0.948 | 0.915 |
| MSNet [42] | 0.755 | 0.678 | 0.041 | 0.737 | **0.883** | 0.836 | 0.907 | **0.862** | 0.028 | 0.893 | 0.944 | 0.922 |
| TGANet [31] | 0.722 | 0.661 | 0.043 | 0.711 | 0.875 | 0.823 | 0.902 | 0.845 | 0.030 | 0.891 | 0.952 | 0.920 |
| LADK [38] | **0.764** | 0.683 | 0.039 | **0.739** | 0.862 | 0.834 | 0.905 | 0.852 | 0.028 | 0.887 | 0.947 | 0.918 |
| M²SNet [41] | 0.758 | **0.685** | **0.038** | 0.737 | 0.869 | **0.842** | **0.912** | 0.861 | **0.025** | **0.901** | **0.953** | 0.922 |
| HCM (Ours) | **0.775** | **0.687** | **0.038** | **0.741** | **0.885** | **0.845** | **0.910** | **0.868** | **0.025** | **0.903** | **0.956** | **0.924** |



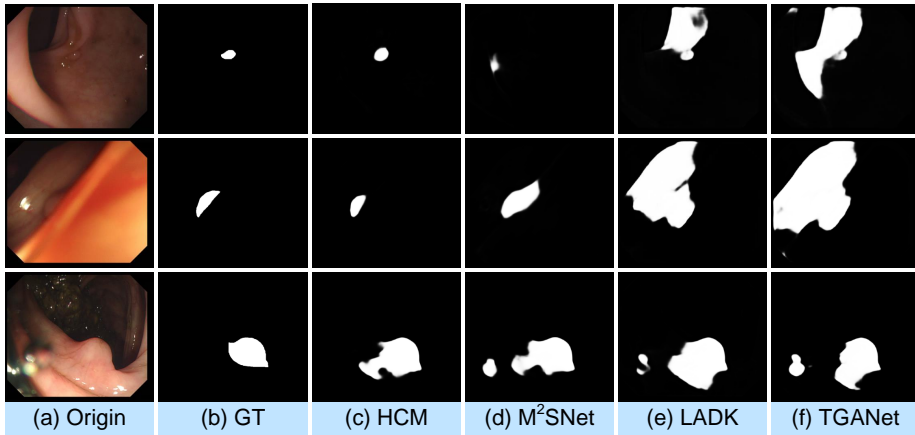(a) Origin    (b) GT    (c) HCM    (d) M²SNet    (e) LADK    (f) TGANet

Fig. 5: Qualitative analysis on the PIS task.

task and present the segmentation results in Table 1. As shown in the table, our HCM outperforms all other segmenters and achieves the top ranking. It surpasses the second-best COD segmenter, SegMaR [17], by a margin of 3.6%. This remarkable performance clearly showcases the superior capability of our HCM in enhancing feature coherence.

**Quanliltative analysis.** As shown in Fig. 4, our HCM demonstrates the capability to generate more complete and comprehensive segmentation results and reduces those uncertainty regions. This improvement can be attributed to our novel hierarchical coherence modeling strategy, which enhances feature coherence within the segmenter. Furthermore, the proposed reversible re-calibration decoder plays a crucial role in enabling the segmenter to effectively identify previously undetected parts within these regions.

## 4.2   Polyp image segmentation

**Datasets and metrics**. In line with the methodology employed in [41], we evaluate the segmentation performance on two widely-used benchmark datasets: CVC-ColonDB and Kvasir. 900 images from Kvasir make up the training set and the testing set comprises the remaining images. Additionally, Consistent with

8      F. Xiao et al.

Table 3: Quantitative comparisons on two benchmarks in transparent object detection. The best two results are in **red** and **blue** fonts.

| Methods | GDD (936 images) | | | | GSD (810 images) | | | |
|---|---|---|---|---|---|---|---|---|
| | mIoU ↑ | $F_\beta^{max}$ ↑ | $M$ ↓ | BER ↓ | mIoU ↑ | $F_\beta^{max}$ ↑ | $M$ ↓ | BER ↓ |
| PMD [20] | 0.870 | 0.930 | 0.067 | 6.17 | 0.817 | 0.890 | 0.061 | 6.74 |
| GDNet [25] | 0.876 | 0.937 | 0.063 | 5.62 | 0.790 | 0.869 | 0.069 | 7.72 |
| GlassNet [19] | 0.881 | 0.932 | 0.059 | 5.71 | 0.836 | 0.901 | 0.055 | 6.12 |
| EBLNet [13] | 0.870 | 0.922 | 0.064 | 6.08 | 0.817 | 0.878 | 0.059 | 6.75 |
| CSNet [1] | 0.773 | 0.876 | 0.135 | 11.33 | 0.666 | 0.805 | 0.135 | 14.76 |
| PGNet [33] | 0.857 | 0.930 | 0.074 | 6.82 | 0.805 | 0.897 | 0.068 | 7.88 |
| GDNet-B [26] | 0.878 | 0.939 | 0.061 | 5.52 | 0.792 | 0.874 | 0.066 | 7.61 |
| ESRNet [21] | 0.901 | 0.942 | 0.046 | 4.46 | 0.854 | 0.911 | 0.046 | 5.74 |
| HCM (Ours) | **0.908** | **0.946** | **0.045** | **4.42** | **0.858** | **0.922** | **0.045** | **5.52** |
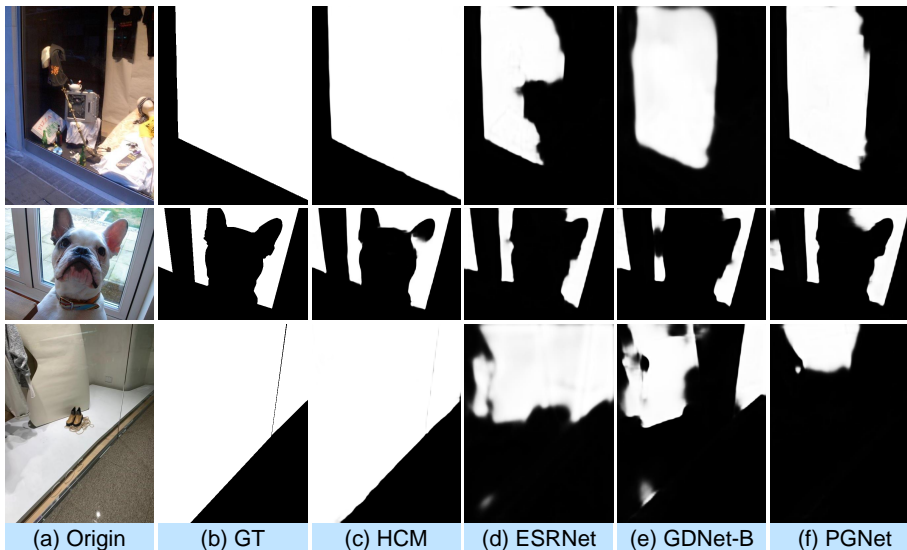


Fig. 6: Qualitative analysis on the TOD task.

[41], we adopt six metrics for quantitative evaluation: namely mean dice (mDice), mean IoU (mIoU), $M$, weighted F-measure ($F_\beta^w$), max E-measure ($E_\phi^{max}$), and $S_\alpha$. For mDice and mIoU, higher values indicate better performance, whereas for the remaining four metrics, higher values indicate poorer performance.

**Quantitative analysis.** Table 2 presents the quantitative comparisons on two benchmarks in polyp image segmentation. As exhibited in Table 2, our proposed HCM outperforms the second-best techniques in 0.6%. This improvement can be attributed to the introduction of our novel modules, namely the Inter-Scale Coherence (ISC) and Contextual Scale Coherence (CSC) modules, which enable the exploration of feature correlations at both single-stage and contextual levels.

**Quanliltative analysis.** As shown in Fig 5, our method can capture polyp more accurately because the proposed HCM method encourages feature coherence, which enables finer discrimination of the gap between foreground and background, leading to improved accuracy in polyp segmentation.

| Metrics | w/o HCM component | w/o RRD | Ours |
|---|---|---|---|
| $M \downarrow$ | 0.035 | 0.033 | **0.032** |
| $F_\beta \uparrow$ | 0.702 | 0.725 | **0.736** |
| $E_\phi \uparrow$ | 0.866 | 0.893 | **0.902** |
| $S_\alpha \uparrow$ | 0.803 | 0.815 | **0.820** |

| Metrics | w/o ISC | w/o CSC | Ours |
|---|---|---|---|
| $M \downarrow$ | 0.033 | 0.033 | **0.032** |
| $F_\beta \uparrow$ | 0.725 | 0.727 | **0.736** |
| $E_\phi \uparrow$ | 0.895 | 0.888 | **0.902** |
| $S_\alpha \uparrow$ | 0.812 | 0.815 | **0.820** |

(a) Break down ablations of HCM.          (b) Effect of the HCM strategy.

Table 4: Ablation study on *COD10K* of the COD task, where "w/o" denotes without. The best results are marked in **bold**.

### 4.3  Transparent object detection

**Datasets and metrics**. In accordance with the experimental setup in [21], we conduct our evaluations on two datasets: *GDD* and *GSD*. To assess the segmentation results, we employ four widely-used metrics: mean intersection over union (mIoU), maximum F-measure ($F_\beta^{max}$), $M$, and balance error rate (BER). The training set consists of 2,980 images from *GDD* and 3,202 images from *GSD*, while the remaining images are allocated to the testing set. It is important to note that a smaller value for $M$ or BER, or a higher value for IoU and $F_\beta^{max}$ indicates superior segmentation performance.

**Quantitative analysis**. Table 3 demonstrates the superior performance of our HCM in transparent object detection (TOD). Our method outperforms the second-best TOD solver, ESRNet, by 1.5%. This substantial improvement further validates the effectiveness and advancement of our proposed HCM segmenter in addressing the challenges of the TOD task.

**Quanliltative analysis**. As depicted in Figure 6, our HCM segmenter achieves more accurate and complete segmentation results compared to the other methods. In contrast, the comparison methods often produce incomplete segments or exhibit blurred parts. These visual comparisons provide compelling evidence of the superiority of our method in addressing the challenges of incomplete segmentation with low-confidence regions.

### 4.4  Ablation Study and Further Analysis

We conduct ablation studies about our HCM on *COD10K* of the COD task.

**Break down ablations of HCM**. As demonstrated in Table 4a, when examining the individual components of our HCM, namely the HCM component or RRD, the performance of HCM decreases. This observation highlights the superiority of our proposed components in contributing to the overall performance of the proposed segmenter.

**Effect of the hierarchical coherence modeling strategy**. We conducted additional experiments to validate the effectiveness of each component in our proposed hierarchical coherence modeling strategy. As shown in Table 4b, our results demonstrate the superiority of the ISC and CSC. These components work in synergy to form a powerful hierarchical coherence modeling strategy.

## 5    Future Work and Conclusions

In our future work, we will consider segmenting concealed objects in those degraded scenarios[8], such as the low-light scenario and the underwater condition[6].

In this paper, we present a novel segmenter called HCM for COS with the aim of addressing the existing limitation of incomplete segmentation. The HCM method focuses on promoting feature coherence by utilizing both intra-stage coherence and cross-stage coherence modules, which explore feature correlations at both the single-stage and contextual levels. Moreover, we introduce the reversible re-calibration decoder to identify previously undetected parts in regions with low-confidence, thereby further improving the segmentation performance. The effectiveness of the proposed HCM segmenter is demonstrated through extensive experiments conducted on three different COS tasks: camouflaged object detection, polyp image segmentation, and transparent object detection. The results obtained from these experiments show promising outcomes, affirming the efficacy of the HCM approach.

# References

1. Cheng, M.M., Gao, S.H., Borji, A., Tan, Y.Q., Lin, Z., Wang, M.: A highly efficient model to study the semantics of salient object detection. IEEE Trans. Pattern Anal. Mach. Intell. **44**(11), 8006–8021 (2021) 8
2. Deng, L., He, C., Xu, G., Zhu, H., Wang, H.: Pcgan: A noise robust conditional generative adversarial network for one shot learning. IEEE Trans. Intell. Transp. Syst. **23**(12), 25249–25258 (2022) 5
3. Fan, D.P., Ji, G.P., Sun, G., Cheng, M.M., Shen, J., Shao, L.: Camouflaged object detection. In: CVPR. pp. 2777–2787 (2020) 2, 4, 5, 6
4. Fan, D.P., Ji, G.P., Zhou, T., Chen, G., Fu, H., Shen, J., Shao, L.: Pranet: Parallel reverse attention network for polyp segmentation. In: MICCAI. pp. 263–273. Springer (2020) 2, 7
5. Fang, Y., Chen, C., Yuan, Y., Tong, K.y.: Selective feature aggregation network with area-boundary constraints for polyp segmentation. In: MICCAI. pp. 302–310. Springer (2019) 7
6. He, C., Fang, C., Zhang, Y., Li, K., Tang, L., You, C., Xiao, F., Guo, Z., Li, X.: Reti-diff: Illumination degradation image restoration with retinex-based latent diffusion model. arXiv preprint arXiv:2311.11638 (2023) 10
7. He, C., Li, K., Xu, G., Yan, J., Tang, L., Zhang, Y., Wang, Y., Li, X.: Hqg-net: Unpaired medical image enhancement with high-quality guidance. IEEE Trans. Neural Netw. Learn. Syst. (2023) 4
8. He, C., Li, K., Xu, G., Zhang, Y., Hu, R., Guo, Z., Li, X.: Degradation-resistant unfolding network for heterogeneous image fusion. In: Proceedings of the IEEE/CVF International Conference on Computer Vision. pp. 12611–12621 (2023) 10
9. He, C., Li, K., Zhang, Y., Tang, L., Zhang, Y., Guo, Z., Li, X.: Camouflaged object detection with feature decomposition and edge reconstruction. In: CVPR (2023) 2, 3, 5
10. He, C., Li, K., Zhang, Y., Xu, G., Tang, L., Zhang, Y., Guo, Z., Li, X.: Weakly-supervised concealed object segmentation with sam-based pseudo labeling and multi-scale feature grouping. NeurIPS (2023) 2
11. He, C., Li, K., Zhang, Y., Zhang, Y., Guo, Z., Li, X., Danelljan, M., Yu, F.: Strategic preys make acute predators: Enhancing camouflaged object detectors by generating camouflaged objects. In: ICLR (2024) 2
12. He, C., Wang, X., Deng, L., Xu, G.: Image threshold segmentation based on glle histogram. In: CPSCom. pp. 410–415. IEEE (2019) 6
13. He, H., Li, X., Cheng, G., Shi, J., Tong, Y., Meng, G., Prinet, V., Weng, L.: Enhanced boundary learning for glass-like object segmentation. In: ICCV. pp. 15859–15868 (2021) 8
14. He, K., Zhang, X., Ren, S., Sun, J.: Deep residual learning for image recognition. In: CVPR. pp. 770–778 (2016) 4
15. Hu, R., Liu, Y., Gu, K., Min, X., Zhai, G.: Toward a no-reference quality metric for camera-captured images. IEEE Trans. Cybern. (2021) 4
16. Hu, R., Liu, Y., Wang, Z., Li, X.: Blind quality assessment of night-time image. Displays **69**, 102045 (2021) 5
17. Jia, Q., Yao, S., Liu, Y., Fan, X., Liu, R., Luo, Z.: Segment, magnify and reiterate: Detecting camouflaged objects the hard way. In: CVPR. pp. 4713–4722 (2022) 2, 6, 7
18. Ju, M., He, C., Liu, J., Kang, B., Su, J., Zhang, D.: Ivf-net: An infrared and visible data fusion deep network for traffic object enhancement in intelligent transportation systems. IEEE Trans. Intell. Transp. Syst. (2022) 5

19. Lin, J., He, Z., Lau, R.W.: Rich context aggregation with reflection prior for glass surface detection. In: CVPR. pp. 13415–13424 (2021) 8
20. Lin, J., Wang, G., Lau, R.W.: Progressive mirror detection. In: CVPR. pp. 3697–3705 (2020) 8
21. Lin, J., Yeung, Y.H., Lau, R.: Exploiting semantic relations for glass surface detection. NIPS **35**, 22490–22504 (2022) 8, 9
22. Lu, Y., He, C., Yu, Y.F., Xu, G., Zhu, H., Deng, L.: Vector co-occurrence morphological edge detection for colour image. IET Image Process. **15**(13), 3063–3070 (2021) 2
23. Lv, Y., Zhang, J., Dai, Y., Li, A., Liu, B., Barnes, N., Fan, D.P.: Simultaneously localize, segment and rank the camouflaged objects. In: CVPR. pp. 11591–11601 (2021) 6
24. Mei, H., Ji, G.P., Wei, Z., Yang, X., Wei, X., Fan, D.P.: Camouflaged object segmentation with distraction mining. In: CVPR. pp. 8772–8781 (2021) 2, 3, 6
25. Mei, H., Yang, X., Wang, Y., Liu, Y., He, S., Zhang, Q., Wei, X., Lau, R.W.: Don't hit me! glass detection in real-world scenes. In: CVPR. pp. 3687–3696 (2020) 2, 8
26. Mei, H., Yang, X., Yu, L., Zhang, Q., Wei, X., Lau, R.W.: Large-field contextual feature learning for glass detection. IEEE Trans. Pattern Anal. Mach. Intell. (2023) 8
27. Oktay, O., Schlemper, J., Folgoc, L.L., Lee, M., Heinrich, M., Misawa, K., Mori, K., McDonagh, S., Hammerla, N.Y., Kainz, B., et al.: Attention u-net: Learning where to look for the pancreas. arXiv preprint arXiv:1804.03999 (2018) 7
28. Pang, Y., Zhao, X., Xiang, T.Z., Zhang, L., Lu, H.: Zoom in and out: A mixed-scale triplet network for camouflaged object detection. In: CVPR. pp. 2160–2170 (2022) 2
29. Rahman, M.A., Wang, Y.: Optimizing intersection-over-union in deep neural networks for image segmentation. In: ISVC. pp. 234–244. Springer (2016) 5
30. Ronneberger, O., Fischer, P., Brox, T.: U-net: Convolutional networks for biomedical image segmentation. In: MICCAI. pp. 234–241. Springer (2015) 7
31. Tomar, N.K., Jha, D., Bagci, U., Ali, S.: Tganet: text-guided attention for improved polyp segmentation. In: MICCAI. pp. 151–160. Springer (2022) 7
32. Wu, Z., Su, L., Huang, Q.: Cascaded partial decoder for fast and accurate salient object detection. In: CVPR. pp. 3907–3916 (2019) 6
33. Xie, C., Xia, C., Ma, M., Zhao, Z., Chen, X., Li, J.: Pyramid grafting network for one-stage high resolution saliency detection. In: CVPR. pp. 11717–11726 (2022) 8
34. Xu, G., He, C., Wang, H., Zhu, H., Ding, W.: Dm-fusion: Deep model-driven network for heterogeneous image fusion. IEEE Trans. Neural Netw. Learn. Syst. (2023) 5
35. Xu, L., Wu, H., He, C., Wang, J., Zhang, C., Nie, F., Chen, L.: Multi-modal sequence learning for alzheimer's disease progression prediction with incomplete variable-length longitudinal data. Med. Image Anal. **82**, 102643 (2022) 5
36. Yang, F., Zhai, Q., Li, X., Huang, R., Luo, A., Cheng, H., Fan, D.P.: Uncertainty-guided transformer reasoning for camouflaged object detection. In: ICCV. pp. 4146–4155 (2021) 2, 6
37. Zhai, Q., Li, X., Yang, F., Chen, C., Cheng, H., Fan, D.P.: Mutual graph learning for camouflaged object detection. In: CVPR. pp. 12997–13007 (2021) 2, 3, 6
38. Zhang, R., Lai, P., Wan, X., Fan, D.J., Gao, F., Wu, X.J., Li, G.: Lesion-aware dynamic kernel for polyp segmentation. In: MICCAI. pp. 99–109. Springer (2022) 7
39. Zhao, J.X., Liu, J.J., Fan, D.P., Cao, Y., Yang, J., Cheng, M.M.: Egnet: Edge guidance network for salient object detection. In: ICCV. pp. 8779–8788 (2019) 6

40. Zhao, T., Wu, X.: Pyramid feature attention network for saliency detection. In: CVPR. pp. 3085–3094 (2019) 6
41. Zhao, X., Jia, H., Pang, Y., Lv, L., Tian, F., Zhang, L., Sun, W., Lu, H.: M2snet: Multi-scale in multi-scale subtraction network for medical image segmentation. IEEE Trans. Med. Imaging (2023) 7, 8
42. Zhao, X., Zhang, L., Lu, H.: Automatic polyp segmentation via multi-scale sub-traction network. In: MICCAI. pp. 120–130. Springer (2021) 7